

Chapter 14

Maximum Likelihood Approach To Estimate The Target Angular Co-Ordinates Under Main Beam Interference Condition: Application To Recorded Live Data

*Alfonso Farina, Giovanni Golino, Luca Timmoneri
afarina@selex-si.com, ggolino@selex-si.com, ltimmoneri@selex-si.com
SELEX-Sistemi Integrati, Rome, Italy*

14.1 Introduction

Modern phased array radars are required to detect, locate and track targets in presence of natural and intentional e.m. interference. Monopulse [14.1] is the conventional technique to determine the target angular coordinates. This technique does not properly work in presence of interference. The intentional interference might impinge on the side lobes as well as on the main beam of the antenna pattern from certain directions. When there is a directional interference in the main beam, it is necessary to use auxiliary antennas which have high gain in the angular region covered by the radar main beam to form a null in the direction of the interference [14.2]. A consequence of this is that the shapes of the sum and difference monopulse beams will be severely distorted by adaptive processing and the conventional monopulse technique can not be applied [14.3].

This chapter illustrates the application of the Maximum Likelihood Estimation (MLE) technique to determine the Target Direction of Arrival (TDoA) in presence of Main Beam Interference (MBI) and the related CRLB (Cramer Rao Lower Bound) angular accuracy. Closed formula for the CRLB of the estimation of TDoA is presented for various interference conditions [14.4]-[14.6].

Two different sets of high gain beams are considered: the first one includes three high gain beams, the sum and the two difference beams (azimuth and elevation). The second set of beams comprises also the so-called double difference beam [14.7].

In this chapter, the following results will be shown:

- conception of the MLE of the target angular co-ordinates (section 14.2),
- closed form expression of the CRLB of the target angular co-ordinates (section 14.3),
- MLE realization via the Newton-Raphson recursion and evaluation of the mean value and of the standard deviation of the estimation errors via Monte Carlo simulation and comparison with the CRLB results (section 14.4),
- test on recorded live data (section 14.5),
- conclusions (section 14.6) and references (section 14.7).

14.2 MLE algorithm for estimation of target angular coordinates

In this section, the MLE of the target angular co-ordinates azimuth and elevation (θ, ϕ) in presence of a directional interference, by processing the data received by a set of high gain beams is presented. The mathematical model of the received radar signals and the processing scheme are detailed.

Let define the vector $\mathbf{v}(\theta, \phi)$ containing the pattern of the antenna beams in a certain direction (θ, ϕ) . We considered two set of beams: the first set is composed by the sum, the difference in azimuth and difference in elevation beams; the second set is composed by the same beams with the addition of the double difference beam. The beams are obtained by a notional two dimensional planar array of 30 by 30 radiating elements spaced of half the transmitting wavelength; C is the carrier frequency. The pattern of such beams are shown in figures 14.1 to 14.4. The -3dB width of the sum beam is 3.5° . The specification on the angular estimator is to achieve an accuracy of one tenth of the -3dB width of the sum beam, thus the standard deviation of the estimation error should not exceed 0.35° .

Figure 14.1: Pattern of the sum beam.

Figure 14.2: Pattern of the difference in azimuth beam

Figure 14.3: Pattern of the difference in elevation.

Figure 14.4: Pattern of the double difference beam.

The set of the received radar echoes can then represent by the following vector:

$$\mathbf{z} \equiv b\mathbf{V}(\theta_r, \phi_r) + \mathbf{d} \quad (14.1)$$

where b is the complex target echo and \mathbf{d} is disturbance, a Gaussian process with zero mean value and covariance matrix \mathbf{M}_d .

The expression of the disturbance covariance matrix is:

$$\mathbf{M}_d = \sigma_n^2 \cdot \left(\mathbf{I} + INR \cdot V(\theta_l, \phi_l) \cdot V(\theta_l, \phi_l)^H \right) \quad (14.2)$$

where (θ_I, ϕ_I) are the angular co-ordinates of the interference and $INR = \frac{P_I}{\sigma_n^2}$ is the interference-to-noise power ratio. (θ_I, ϕ_I) are the angular coordinates of the interference.

Owing to the Gaussian nature of the pdf of \mathbf{z} , the MLE problem brings to the following minimisation problem:

$$\left(\hat{b}, \hat{\theta}_T, \hat{\phi}_T\right) = \arg \min_{b, \theta, \phi} \left\{ \left[\mathbf{z} - b\mathbf{V}(\theta, \phi) \right]^H \mathbf{M}_d^{-1} \left[\mathbf{z} - b\mathbf{V}(\theta, \phi) \right] \right\} = \arg \min_{b, \theta, \phi} F(b, \theta, \phi) \quad (14.3)$$

The minimisation of the above-mentioned functional corresponds also to the maximisation of following functional:

$$Q(\theta, \phi) = \frac{\left| \mathbf{V}^H(\theta, \phi) \cdot \mathbf{M}_d^{-1} \cdot \mathbf{z} \right|^2}{\mathbf{V}^H(\theta, \phi) \cdot \mathbf{M}_d^{-1} \cdot \mathbf{V}(\theta, \phi)} \quad (14.4)$$

that is the one used in the following.

The algorithm needs the estimation of the disturbance covariance matrix, which is obtainable by the echoes corresponding to range cells adjacent to the cell under test. In the simulations of section 14.4 and in the test on live data of section 14.5 we considered 15 range cells. Also we need the description of the quiescent beam shapes in the main beam region; these are available from the antenna design and measurements.

The maximum of the functional can be estimated by an exhaustive search in the range of values of interest or by using a fast recursive algorithm, like the Newton-Raphson one:

$$\hat{\mathbf{x}}_{k+1} = \hat{\mathbf{x}}_k - \left[E \left\{ \frac{\partial^2 Q}{\partial \mathbf{x}^2} \bigg|_{\hat{\mathbf{x}}_k} \right\} \right]^{-1} \left[\frac{\partial Q}{\partial \mathbf{x}} \bigg|_{\hat{\mathbf{x}}_k} \right] \quad (14.5)$$

where $\hat{\mathbf{x}}_k = [\hat{\theta}_k \ \hat{\phi}_k]^T$. The recursion can be initialized as with the angular coordinates of the main beam pointing.

Moreover the comparison of the Q functional with a suitable threshold λ permits the target detection maintaining the prescribed constant false alarm rate. Only for the range cell in which the detection occurred, the radar signals are taken and further processed by the MLE algorithm to produce the target DoA.

In figure 14.5 a flow chart of the processing chain is shown.

Figure 14.5: Flow chart of processing chain.

14.3 CRLB of estimation of target angular coordinates

To calculate the CRLB, the Fisher Information Matrix (FIM) is needed; its definition is as follows [14.8]:

$$\mathbf{FIM} = E \left\{ \begin{bmatrix} \frac{\partial^2 F}{\partial \theta^2} & \frac{\partial^2 F}{\partial \theta \partial \phi} & \frac{\partial^2 F}{\partial \theta \partial b_r} & \frac{\partial^2 F}{\partial \theta \partial b_i} \\ \frac{\partial^2 F}{\partial \phi \partial \theta} & \frac{\partial^2 F}{\partial \phi^2} & \frac{\partial^2 F}{\partial \phi \partial b_r} & \frac{\partial^2 F}{\partial \phi \partial b_i} \\ \frac{\partial^2 F}{\partial b_r \partial \theta} & \frac{\partial^2 F}{\partial b_r \partial \phi} & \frac{\partial^2 F}{\partial b_r^2} & \frac{\partial^2 F}{\partial b_r \partial b_i} \\ \frac{\partial^2 F}{\partial b_i \partial \theta} & \frac{\partial^2 F}{\partial b_i \partial \phi} & \frac{\partial^2 F}{\partial b_i \partial b_r} & \frac{\partial^2 F}{\partial b_i^2} \end{bmatrix} \right\} \quad (14.6)$$

where b_r and b_i are the real part and the imaginary parts of the target echo.

The CRLB values for the standard deviation of the estimates of the azimuth and elevation coordinates of the target are obtained by the following formulas:

$$\begin{aligned} \sigma_\theta &= \sqrt{[\mathbf{FIM}^{-1}]_{1,1}} \\ \sigma_\phi &= \sqrt{[\mathbf{FIM}^{-1}]_{2,2}} \end{aligned} \quad (14.7)$$

In this section, the following scenario is considered for the analysis: one main beam interference with INR (Interference-to thermal-noise power ratio) = 30 dB set in $(\theta_i, \phi_i) = (-1.5^\circ, -1.5^\circ)$ and a target with SNR (Signal-to thermal-noise power ratio) = 30 dB having its angular coordinates a changing parameter.

To simulate the detection process, the false alarm probability has been set to 10^{-6} , and the required detection probability has been set to 80%.

In figure 14.6 the target angular sectors in which the requirements on the detection probability and on the CRLB are satisfied using the three beams set are shown. The requirement on the CRLB is satisfied only in a little area around the interference, but in almost all the sector the target is not

detectable. Therefore when the target is detectable with the required probability, its position cannot be estimated with satisfactory accuracy.

Figure 14.6: Areas where the probability of detection and the CRLB of the angular accuracy satisfy the requirements ($P_d > 0.8$; $CRLB < 0.35^\circ$) for the set of three high gain beams.

In figure 14.7 the target angular sectors for which the requirements on the detection probability and on the CRLB are satisfied using the four beams set are shown. In most part of the sectors, both the two requirements are satisfied. Around the interference position it is still not possible to detect the target. The target is detectable with the required probability and its position can be estimated with the needed accuracy if the separation of the target in azimuth and in elevation from the interference is more than 0.5° .

Figure 14.7: Areas where the probability of detection and the CRLB of the angular accuracy satisfy the requirements ($P_d > 0.8$; $CRLB < 0.35^\circ$) for the set of four high gain beams.

In the following four figures more details about the CRLB curves are displayed.

In figures 14.8 and 14.9 the CRLB of the azimuth estimation as function of the target azimuth is shown respectively for the three beam set and for the four beam set. The minimum of the curves is obtained for the interference azimuth and it is independent of the target elevation angle and of the number of beams used by the algorithm. For the other target azimuth values, the CRLB of the four

beam set is smaller than the three beam set one; the four beam curves are much flat than the three beam curves.

Figure 14.8: CRLB of the azimuth angular accuracy vs. the azimuth of the target for the set of three high gain beams. Different values of the elevation of the target.

Figure 14.9: CRLB of the angular accuracy vs. the azimuth of the target for the set of four high gain beams. Different values of the elevation of the target.

In figures 14.10 and 14.11 the CRLB of the azimuth estimation as function of the target elevation is shown respectively for the three beam set and for the four beam set. If the target and interference elevation coincide, the values of the CRLB is independent of the number of beams used by the algorithm and they are point of maxima for the four beam set. For the other target elevation values, the CRLB of the four beam set is much smaller than the three beam set.

Figure 14.10: CRLB of the azimuth angular accuracy vs. the elevation of the target for the set of three high gain beams. Different values of the azimuth of the target.

Figure 14.11: CRLB of the azimuth angular accuracy vs. the elevation of the target for the set of four high gain beams. Different values of the azimuth of the target.

14.4 MLE algorithm simulation results

The MLE algorithm has been tested for different target positions. The results have been obtained by averaging 100 independent Monte Carlo trials. The results have been summarized and compared to the corresponding CRLB values in Table 14.1. The target has been always detected in all the trials.

Table 14.1 : Results of the MLE algorithm simulation; scenario consisting of a target with angular co-ordinates (θ_T, ϕ_T) and of a MBI with co-ordinates $(\theta_T, \phi_T) = (-1.5^\circ, -1.5^\circ)$; SNR=INR=30 dB; results averaged over 100 Monte Carlo trials; the target has been detected in all the trials

The standard deviation of the target azimuth and elevation estimated by using three beams has been always unsatisfactory, as expected, by checking the corresponding CRLB values. Moreover, the estimation of the coordinates is not always unbiased and its standard deviation sensibly exceeds the corresponding CRLB value.

The standard deviation of the target azimuth and elevation estimated by using four beams instead fulfils the requirements and it is practically coincident with the corresponding CRLB values. Moreover, the estimation of the coordinates is always unbiased.

Figures 14.12 and 14.13 show two examples of estimation of the Q function (see eq. (14.4)) on which the MLE algorithm is based. The scenario is the same in both figures (SNR=INR=30 dB,

$(\theta_T, \phi_T) = (-1.5^\circ, -1.5^\circ)$, $(\theta_T, \phi_T) = (+1^\circ, +1^\circ)$, figure 14.12 is referred to the three beam case, while figure 14.13 to the four beam case.

Figure 14.12: Estimation of the Q function (averaged over 100 Monte Carlo trials) with three beams; the target position is marked as a triangle and the interference position as a square.

Figure 14.13: Estimation Q function (averaged over 100 Monte Carlo trials) with four beams; the target position is marked as a triangle and the interference position as a square.

Both the functions have a maximum in the target position and a “spiky” minimum in the interference position. The width of the maximum is an indicator of the accuracy of the angular estimation. The maximum of the four beam case is in fact much narrower than the case of three beams and indicates a much better accuracy. In the same way the “spiky” minima indicate that the MLE algorithm can in addition provide in both cases an accurate estimation of the interference position.

14.5 Test on recorded live data

To test the validity of the MLE approach, several sets of data have been recorded in a site with a ground based test bed C-band phased array radar (C-PAR) equipped with three high gain beams [14.9], [14.10].

The purpose of this section is to analyze the performance of the MLE algorithm to estimate the target angular co-ordinates in presence of an MBI on the C-PAR recorded real data. After a brief description of the experimental set-up, the subsequent items are discussed:

- firstly a comparison between the beams reconstructed by simulation and the C-PAR real ones is performed;
- secondly a suitable phase compensation on the reconstructed beams is estimated to make them congruent with the real ones; then the estimates of the target co-ordinates, obtained after such compensation, are compared to the uncompensated ones;
- an estimate of the interference position has been performed using the same MLE algorithm, and the estimates with and without phase compensation are compared; the congruence of the reconstructed scenario obtained by the compensated estimates has been analyzed and compared to the target and interference real positions.

14.5.1 Description of the radar for data capture

The radar used for the live data capture was a test bed passive phased array C-band radar equipped with a multi channel digital data recorder (MDDR) to acquire simultaneously the live data from three receiving channels. Its three receiving channels allowed the data recording from the sum, difference in elevation and difference in azimuth beams. It was also possible to install two low gain auxiliaries at the extremities of the main antenna to test the sidelobe canceller (SLC) and the sidelobe blanker (SLB) [14.2], [14.9], [14.10]. In a phase of the experiments, it was also possible to acquire data from the sum channel, one of the two difference channels and one of the two low gain auxiliary channels to test the radar in a mixture of mainbeam and sidelobe interference conditions. During the interference acquisition campaign, several recordings were made with the aim of testing the performance of MLE algorithms for TDoA estimation.

14.5.2 Data capture experimental set up

A series of trials was performed to evaluate the performance of the C-PAR under various scenarios. A set of suitably positioned interference emulators and transponders were used to produce the required scenario and the antenna was pointed either electronically or manually in the direction of the required interference emitter. Figure 14.14 depicts the environmental set up.

Figure 14.14. Experimental set up.

Two transponders (TP1 and TP2) emulated the useful targets; three interference emulators (IE1, IE2 and IE3) were also present to test the performance of the radar in various conditions to achieve the following goals:

- characterisation of radar receiving channels, cancellation of two contemporaneous continuous Noise-Like Interference (NLI),
- one NLI impinging on the main antenna beam,
- cancellation of two contemporaneous continuous NLI with angular distance either less than the radar beamwidth or wider,
- detection of target in presence of two contemporaneous continuous NLIs,
- blanking probability in presence of Coherent Repeater Interference (CRI) only,
- blanking of CRI and cancellation of NLI,
- contemporaneous cancellation of jamming and clutter via STAP (Space-Time Adaptive Processing) algorithms,

- MLE estimation of TdoA under main beam jamming conditions.

Live data were acquired soon after the A/D (Analogue-to-Digital) converters by means of the MDDR permitting the simultaneous recording on the three receiving channels. Approximately 3 Gigabytes of data have been successfully collected.

14.5.3 Comparison between the theoretical and real radar beams

A discrepancy has been found between the phase of the “difference and sum C-PAR beams ratio” that has been simulated and the real C-PAR one found during the data recordings. The confirmation of such hypothesis could negatively influence the accuracy of the angular estimate based on the MLE algorithm described in the previous section 2. The algorithm can correctly estimate the target angular co-ordinates from real data provided that it uses a good approximation of beam patterns from which the data were acquired.

In Figures 14.15 and 14.16 the phase diagrams of the ratio between the simulated difference in azimuth and sum beams and of the ratio between the simulated difference in elevation and sum beam are shown, respectively for the 0° elevation and the 0° azimuth planes. These plots are independent, with a good approximation, respectively on the considered elevation and azimuth angles; they can be considered valid also for the other constant elevation and azimuth planes.

Figure 14.15. Phase diagrams of the simulated ratio between the difference in azimuth and sum beams vs. the azimuth angle. The elevation angle is 0° .

Figure 14.16. Phase diagrams of the ratio between the simulated difference in elevation and sum beams vs. the elevation angle. The azimuth angle is 0° .

In Figure 14.15, the phase of the ratio between the difference in azimuth and the sum beams is 107.5° for the positive values of the azimuth, it is -72.5° for the negative ones. In Figure 14.16, the phase of the ratio between the difference in elevation and the sum beams is -90.8° for the positive values of the elevation, it is 89.6° for the negative ones. The phase step is in both cases 180° , as the theory requires.

The file P90803k has been considered for a first evaluation of the phases of the ratio between the difference and sum C-PAR beams. In this file, the signals received by the sum, the difference in azimuth and the difference in elevation beams of the C-PAR have been recorded. The scenario included a target (simulated by the transponder TP2 in Figure 14.14) and an MBI (simulated by the transmitting antenna IE1 in Figure 14.14). The sweeps corresponding to the 1st and 19th PRT (Pulse Repetition Time) with 1134 range samples have been considered.

To calculate the phases of the ratio between the difference and the sum beams, the samples from the 600th range cell to the 700th range cell (in which only the interference is present) have been considered, for both the 1st and the 19th PRTs. The results are shown in Figures 14.17 to 14.20 (the phases are module 2π).

Figure 14.17. Phase of the ratio between the difference in azimuth and the sum beams; file P90803k, 1st PRT with 1134 range samples.

Figure 14.18. Phase of the ratio between the difference in elevation and the sum beams; file P90803k, 1st PRT with 1134 range samples.

Figure 14.19. Phase of the ratio between the difference in azimuth and the sum beams; file P90803k, 19th PRT with 1134 range samples.

Figure 14.20. Phase of the ratio between the difference in elevation and the sum beams; file P90803k, 19th PRT with 1134 range samples.

The phases are not constant, but they have some oscillations due to slight variation of the INR from sample to sample. Furthermore, it can be noted that the value of the phase of the ratio between the signal received on the difference in azimuth channel and the signal on the sum sensibly changes passing from the 1st to the 19th PRTs (from about -150° to 30° , with a variation of 180°); this can happen if the interference has passed through the null of the difference in azimuth beam during the antenna rotation. The phase of the ratio between the signal received by the difference in azimuth channel and the signal received by the sum, therefore, has a 180° step after the interference has passed through the null, as the theory requires. The phase of the ratio between the signal received by the difference in elevation channel and the signal received by the sum, instead, remains practically constant, except for a soft ripple due to the noise.

Concluding, from the results obtained by the recordings it appears evident there is some difference between the phase of the simulated beams and the phase of the C-PAR beams. This fact could deteriorate the angle estimation accuracy unless a suitable phase match between the simulated

beams (the ones exploited by the MLE algorithm) and the C-PAR beams on the two difference channels is made.

14.5.4 MLE on recorded live data

Using the figures 14.17 to 14.20, the phase of the ratio between the difference in azimuth and sum beams has been estimated equal to -150° ; it has been supposed that the interference had positive azimuth co-ordinate during the considered recording; thus, a phase shift of -260° has been provided to the reconstructed difference in azimuth beam for matching it to the C-PAR one. Moreover, the phase of the ratio between the difference in elevation and sum beams in the C-PAR case has been estimated equal to -70° ; it has been supposed that the interference had positive elevation during the considered recording, thus a phase shift of $+20^\circ$ has been provided to the reconstructed difference in elevation beam.

Figures 14.21 and 14.22 portray the achieved results obtained with the phase compensation. The estimations obtained with the phase compensation seem more reliable. Infact the antenna was rotating in azimuth clockwise with a constant elevation angle.

Figure 14.21. Estimate of the target azimuth; file P90803k, PRT with 1134 range samples, phase compensation.

Figure 14.22. Estimate of the target elevation; file P90803k, PRT with 1134 range samples, phase compensation.

14.6 Conclusions

The increase of the number of degrees of freedom from three to four greatly improves the accuracy of the MLE of the TDoA in presence of one MBI also when the SNR is comparable to INR. If the both target and jammer coordinates are not too close, the MLE with the selected four beams set (sum, difference in azimuth, difference in elevation, double difference) is able to estimate the target angular coordinates with the required accuracy. Therefore, this estimate is very close to the correspondent CRLB.

From the test on live data, it has been found that the MLE of TDoA in presence of MBI needs the knowledge of the amplitude and phase patterns of the antenna beams to properly work. The analysis of the recorded real data has shown that the estimates are very sensible to possible inaccuracies in the reconstructed patterns. This problem has been tackled by obtaining an approximate estimate of the phase characteristics of the antenna patterns. It has been demonstrated that the algorithm provides reliable estimates of the target angular co-ordinates in presence of one MBI.

14.7 References

[14.1] M. I. Skolnik, "Radar Handbook", 2nd edition, Mc Graw Hill, 1990 (ch. 18).

[14.2] A. Farina: "Antenna Based Signal Processing Techniques for Radar Systems", Artech House, 1992.

[14.3] P. Langsford, A. Farina, L. Timmoneri, R. Tosini, "Monopulse direction finding in presence of adaptive nulling". IEE Colloquium, 'Advances in Adaptive Beamforming', 13 June 1995, Romsey (UK).

- [14.4] M. Valeri, S. Barbarossa, A. Farina, L. Timmoneri, "Monopulse estimation of target DoA in external fields with adaptive arrays". 1996 IEEE Symposium of Phased Array Systems and Technology, 15-18 October, 1996, Boston (MA), pp. 386-390.
- [14.5] A. Farina, G. Golino, L. Timmoneri, "Maximum likelihood approach to the estimate of target angular co-ordinates under a main beam interference condition", CIE 2001 International Conference on Radar, October 15-18, 2001, Beijing China, pp. 834-838. Invited lecture.
- [14.6] A. Farina, P. Lombardo, L. Ortenzi, "A Unified Approach to Adaptive Radar Processing with General Antenna Array Configuration", "Special Issue on New Trends and Findings in Antenna Array Processing for Radar", Signal Processing, 84, September 2004, pp. 1593-1623, Elsevier.
- [14.7] J. B. Hoffman, B.L. Gabelach, "Four-Channel Monopulse for Main Beam Nulling and Tracking", Proc. of IEEE National Radar Conference NATRAD '97, May 13-15, 1997, Syracuse, New York, pp. 94-98.
- [14.8] S. Kay, "Fundamentals of Statistical Signal Processing: Estimation Theory", Prentice Hall, 1993.
- [14.9] A. Farina, L. Timmoneri, "Cancellation of clutter and e.m. interference with STAP algorithms. Application to live data acquired with a ground-based phased-array radar demonstrator". 2004 IEEE Radar Conference, Philadelphia (USA), pp. 486-491.
- [14.10] A. Farina, G. A. Fabrizio, W. L. Melvin, L. Timmoneri, "Multichannel array processing in radar: state of the art, hot topics and way ahead". Invited paper, IEEE Sensor and Multichannel Array Processing (SAM04) workshop, July 18, 2004 to July 21, 2004 in Sitges.

Alfonso Farina (Fellow of IEEE and Fellow of IEE) received his doctor degree in electronic engineering from the University of Rome (I) in 1973. In 1974 he joined Selenia, now Alenia Marconi Systems, where he is a manager (since May 1988); since one year he is a member of the Chief Technical Office. Recently he has been appointed Scientific Director. In his professional life Alfonso has provided technical contributions to detection, signal, data & fusion, image processing for radar systems. He has provided leadership in many projects – also conducted in the international arena – in surveillance for ground and naval applications, in airborne early warning and in imaging radar. Since 1979, he has also been *Professore Incaricato* of Radar Techniques at the University of Naples; in 1985 he was appointed Associate Professor. He is the author of more than 330 peer reviewed publications and the author of books and monographs: *Radar Data Processing (Vol. 1 and 2) (translated in Russian and Chinese), 1985-1986 ; Optimised Radar Processors, 1987 ; Antenna Based Signal Processing Techniques for Radar Systems, 1992*. He has written the Chapter 9 on “ECCM techniques” in the Radar Handbook (2nd Edition 1990), edited by Dr. M. I. Skolnik of Naval Research Laboratory. He has been session chairman at many international radar conferences. He uses to lecture at universities and research centres in Italy and abroad; He also frequently gives tutorials at the Intl. Radar Conferences on signal, data and image processing for radar; in particular on multi-sensor fusion, adaptive signal processing, space time adaptive processing (STAP) and detection. In the 1987 He received the Radar Systems Panel Award of IEEE-AESS *for development of radar data processing techniques*. He is the Italian representative at the International Radar Systems Panel of IEEE-AESS. He has been the Italian industrial representative at the SET (Sensor and Electronic Technology) of RTO (Research Technology Organisation) of NATO. He has been in the BoD of the International Society for Information Fusion (ISIF). He has been nominated Fellow of IEEE with the following citation: *"For development and application of adaptive signal processing methods for radar systems."* He is a referee of numerous publications submitted to several Journals of IEEE, IEE, Elsevier, etc., He has also cooperated with the editorial board of ECEJ (Electronics & Communication Engineering

Journal) of IEE. More recently, Alfonso serves as a member in the Editorial Board of Signal Processing (Elsevier). He is the co-recipient of the prestigious best paper award, entitled to Mr. B. Carlton, of IEEE Trans. on Aerospace and Electronic Systems for the year 2001. Alfonso has been the leader of the team that received the 2002 AMS CEO award for Innovation Technology. Moreover, Alfonso has been the co-recipient of the AMS Radar Division award for Innovation Technology in 2003. Recently, He has been the leader of the team that has won in 2004 the 1st prize award for Innovation Technology of Finmeccanica. Finmeccanica (Italy) is the holding of 16 Companies (including AMS) with 46000 employees. This award context has seen the submission of more than 320 projects. This prestigious award has been set for the first time in 2004. Recently, Alfonso has been appointed as NATO-SET (Sensor and Electronic Technology) Panel Member at Large.

Giovanni Golino received his doctor degree in electronic engineering from the University of Rome (II) in 1998. In 1999 he joined AMS, where he is a Radar Designer in the Radar and Technology & Operation Division, Systems Analysis Group. His actual areas of investigation are high resolution radars, ECCM techniques and systems of sensors.

Luca Timmoneri received the doctor degree in electronic engineering from the University of Rome, Italy, in 1989. In 1989 he joined Selenia S.p.A. now AMS (Alenia Marconi Systems), where he is currently the Head of the Radar System Analysis Group of the Radar and Technology Division. His working interests span from the area of synthetic aperture radar (image formation and moving target detection and imaging), to space-time adaptive processing for AEW and ground-based radar, to parallel processing architectures with VLSI and COTS devices. He is presently involved in the areas of adaptive signal processing, detection and estimation with application to tri-dimensional ground and ship based phased array radar. He is the author of several peer reviewed papers (also invited) on journals and conference proceedings. He is the co-author of three tutorials

on adaptive array and space-time adaptive processing presented at the intl. IEEE radar conference in Washington DC (1995) , Boston (1999) and Boston (2003). Dr. Timmoneri received the 2002 AMS CEO Award, the 2003 AMS MD Award, the 2004 AMS CEO Award for Innovation Technology, and the 1st prize award for Innovation Technology of Finmeccanica 2004.

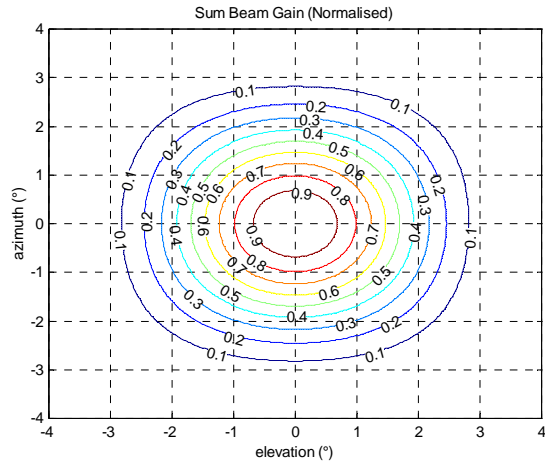


Figure 14.14: Pattern of the sum beam.

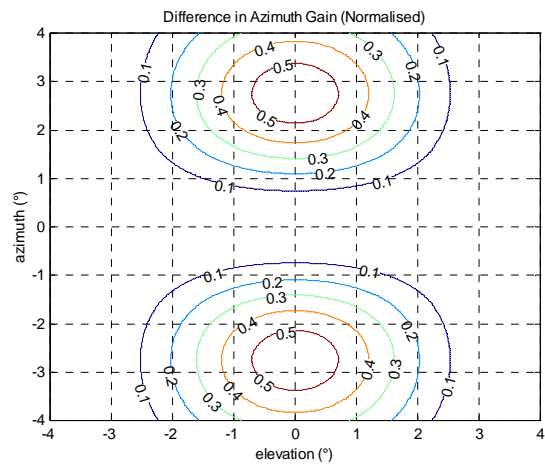


Figure 14.15: Pattern of the difference in azimuth beam.

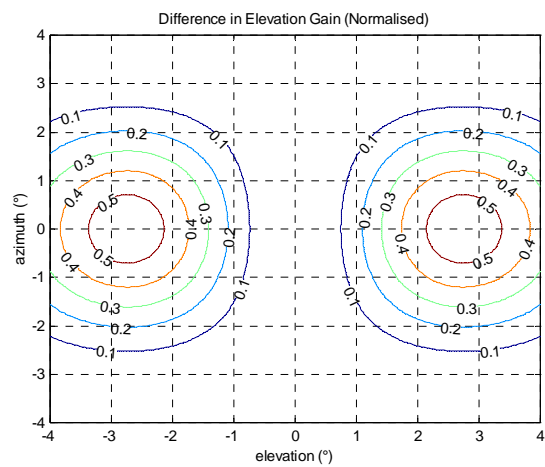


Figure 14.16: Pattern of the difference in elevation.

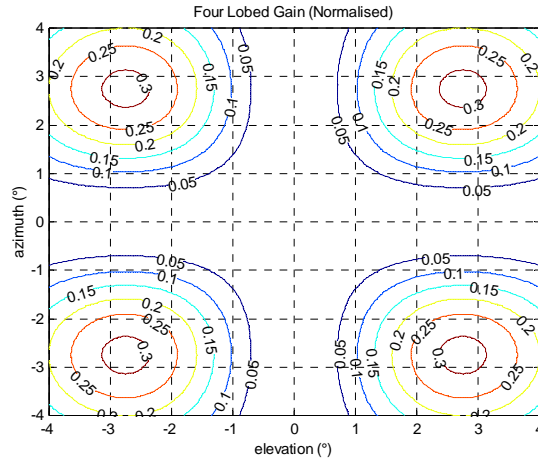


Figure 14.17: Pattern of the double difference beam.

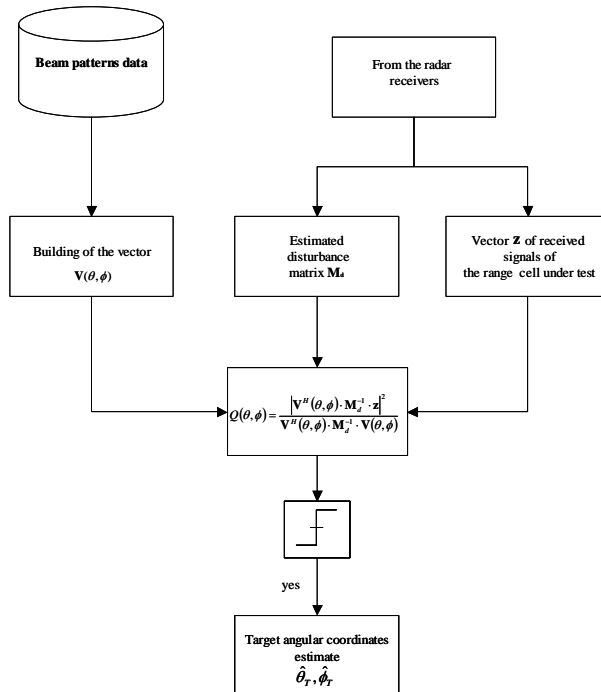


Figure 14.18: Flow chart of processing chain.

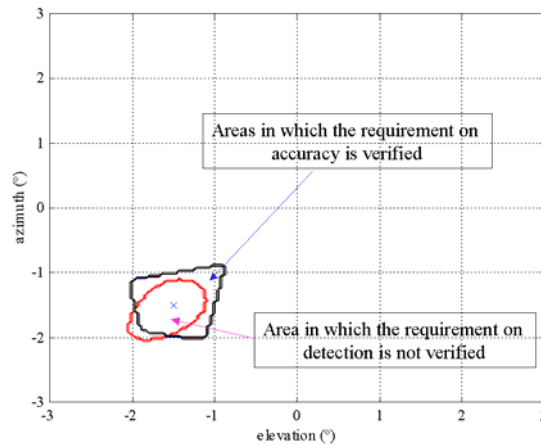


Figure 14.19: Areas where the probability of detection and the CRLB of the angular accuracy satisfy the requirements ($P_d > 0.8$; $CRLB < 0.35^\circ$) for the set of three high gain beams.

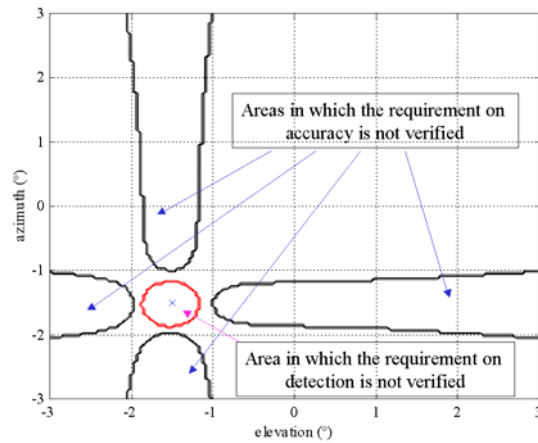


Figure 14.20: Areas where the probability of detection and the CRLB of the angular accuracy satisfy the requirements ($P_d > 0.8$; $CRLB < 0.35^\circ$) for the set of four high gain beams.

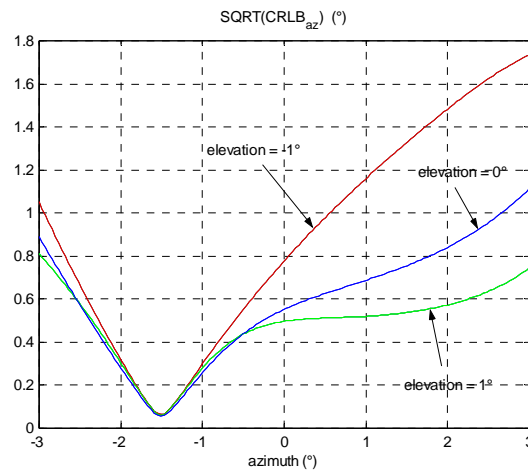


Figure 14.21: CRLB of the azimuth angular accuracy vs. the azimuth of the target for the set of three high gain beams. Different values of the elevation of the target.

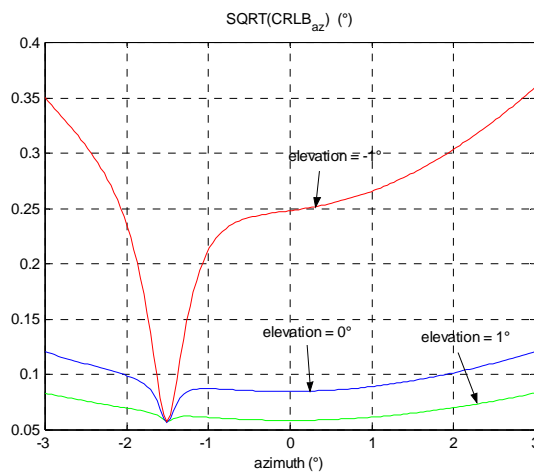


Figure 14.22: CRLB of the angular accuracy vs. the azimuth of the target for the set of four high gain beams. Different values of the elevation of the target.

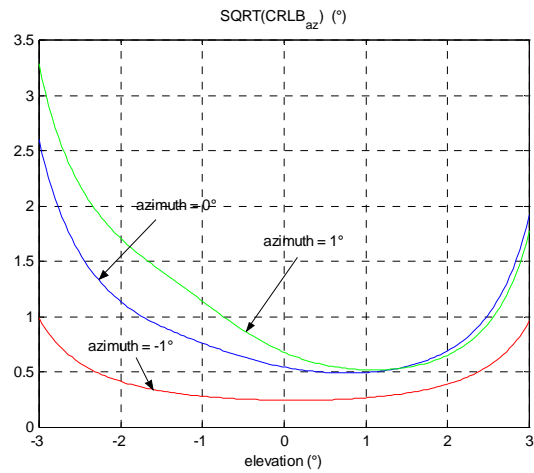


Figure 14.23: CRLB of the azimuth angular accuracy vs. the elevation of the target for the set of three high gain beams. Different values of the azimuth of the target.

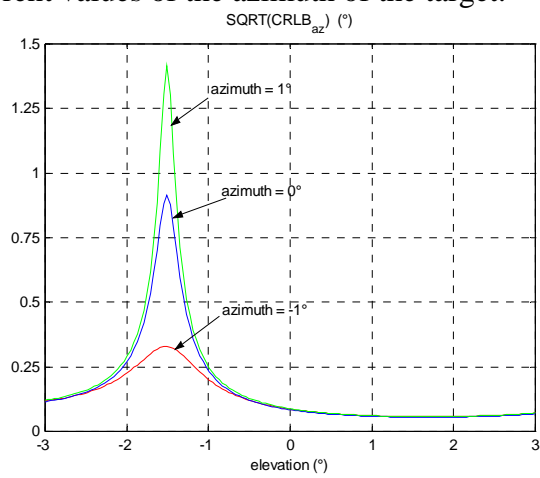


Figure 14.24: CRLB of the azimuth angular accuracy vs. the elevation of the target for the set of four high gain beams. Different values of the azimuth of the target.

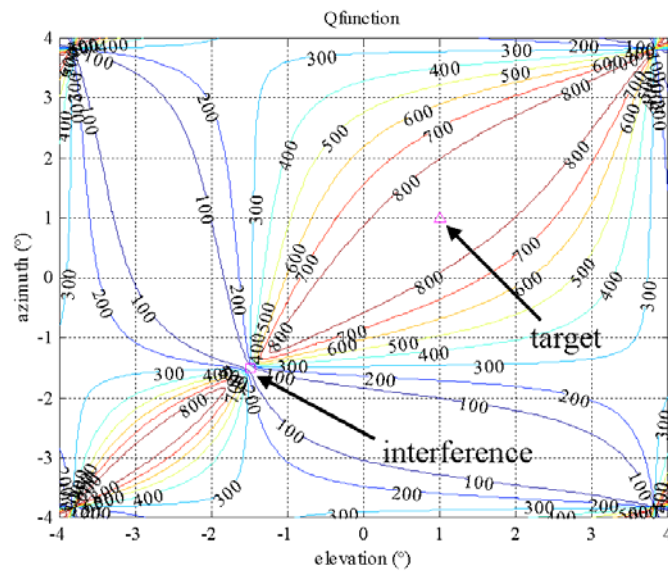


Figure 14.25: Estimation of the Q function (averaged over 100 Monte Carlo trials) with three beams; the target position is marked as a triangle and the interference position as a square.

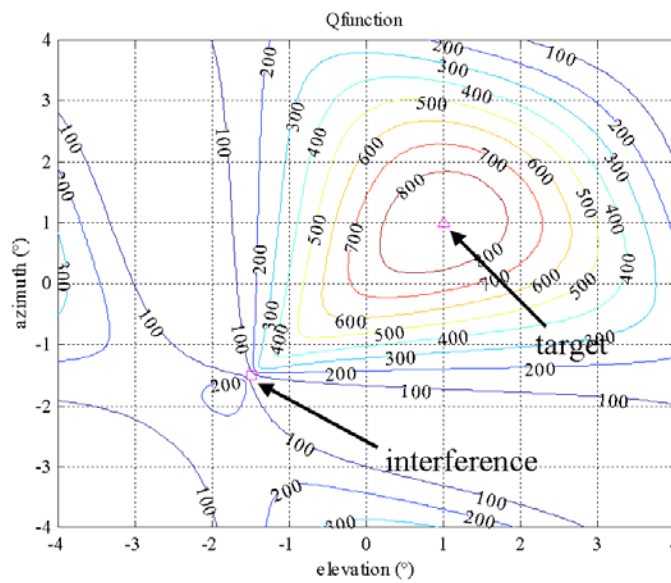


Figure 14.26: Estimation Q function (averaged over 100 Monte Carlo trials) with four beams; the target position is marked as a triangle and the interference position as a square.

3D view of the experimental configuration

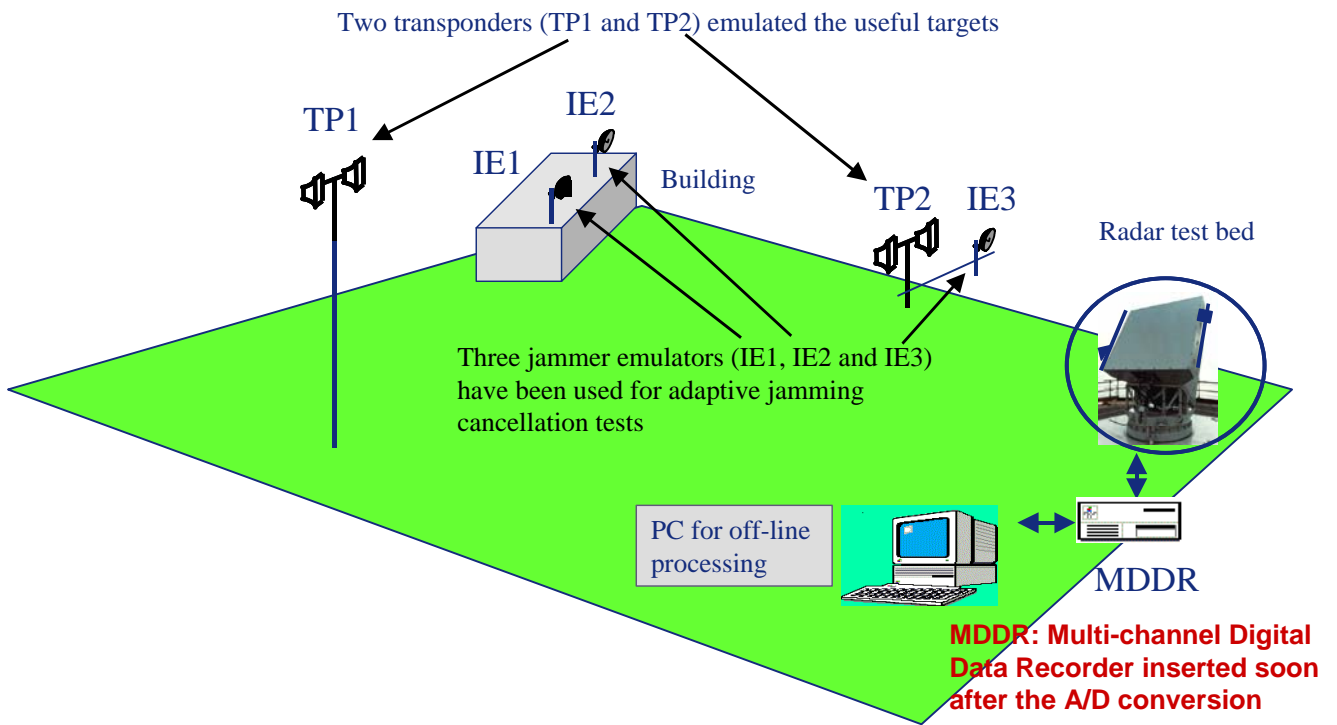


Figure 14.14. Experimental set up.

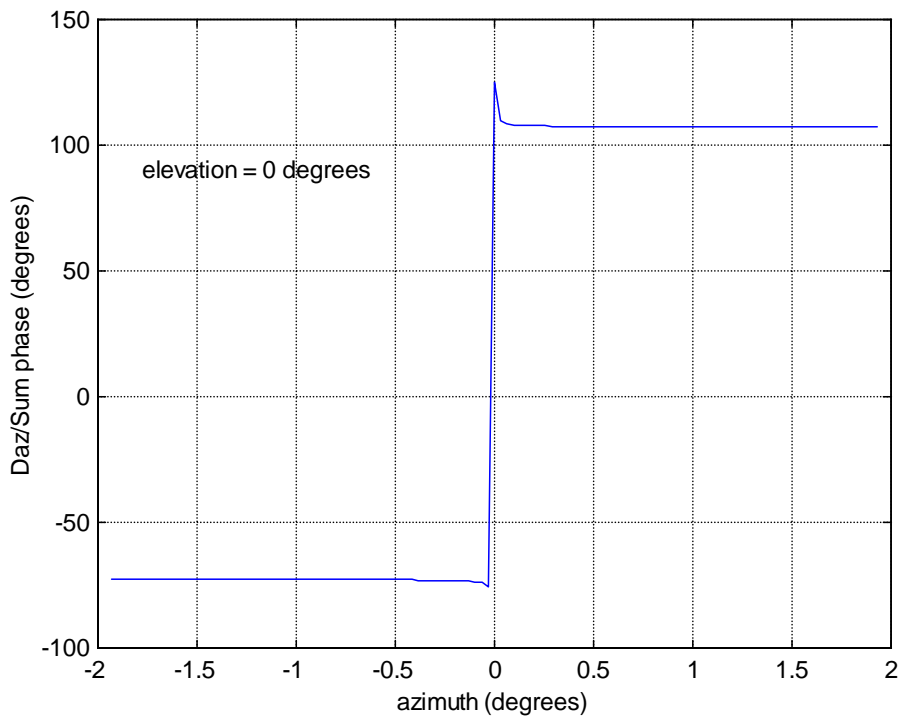


Figure 14.15. Phase diagrams of the simulated ratio between the difference in azimuth and sum beams vs. the azimuth angle. The elevation angle is 0° .

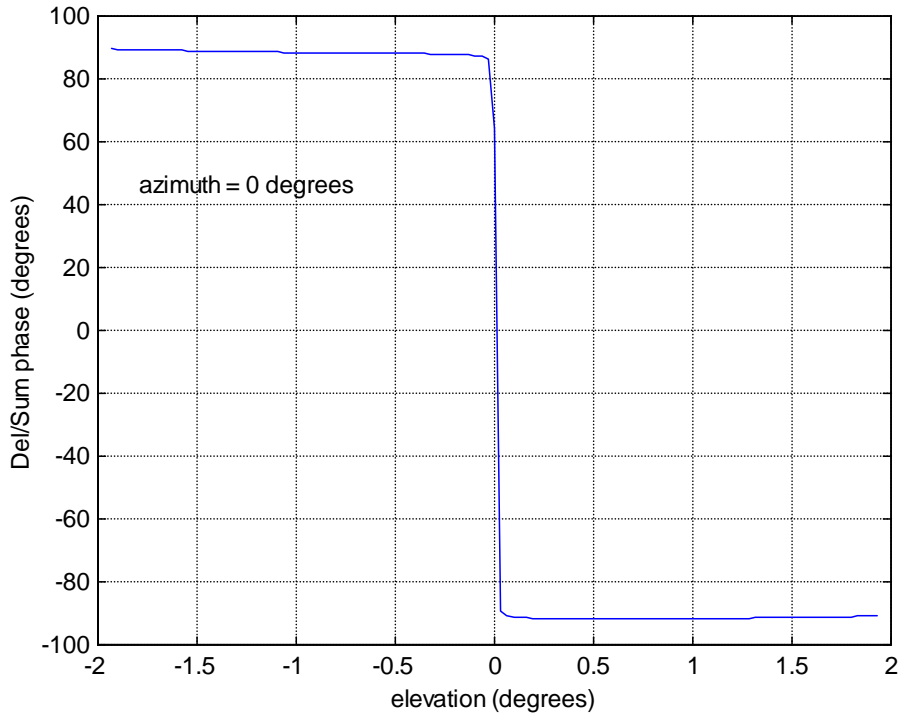


Figure 14.16. Phase diagrams of the ratio between the simulated difference in elevation and sum beams vs. the elevation angle. The azimuth angle is 0° .

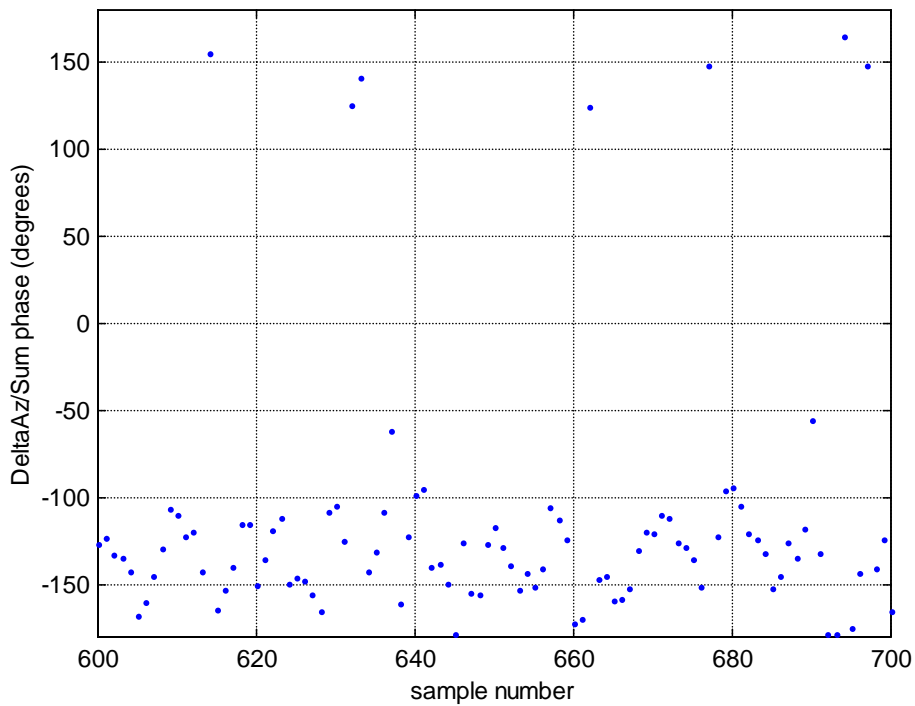


Figure 14.17. Phase of the ratio between the difference in azimuth and the sum beams; file P90803k, 1st PRT with 1134 range samples.

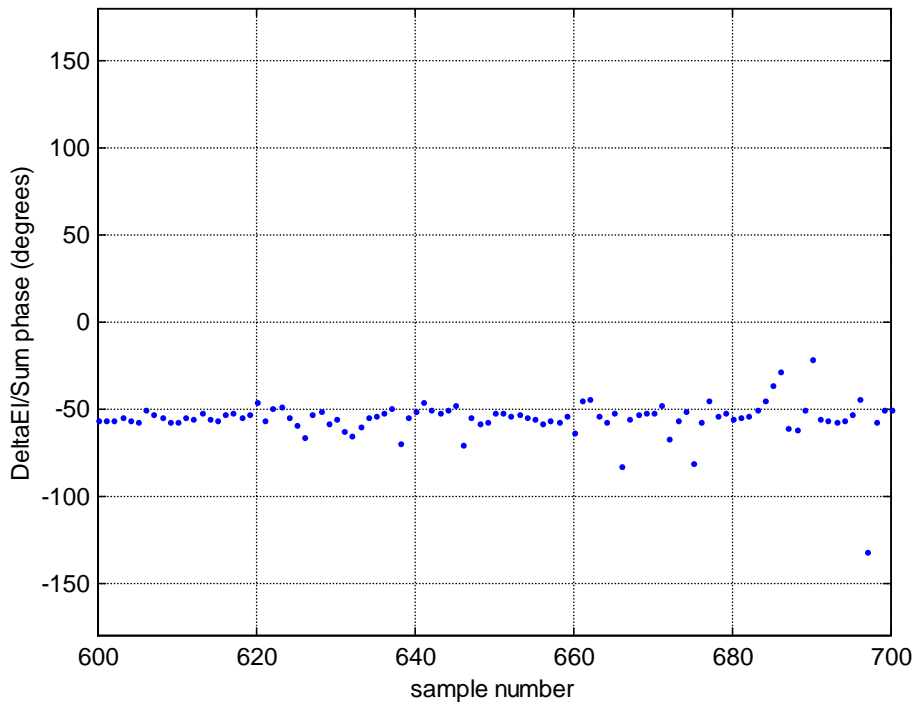


Figure 14.18. Phase of the ratio between the difference in elevation and the sum beams; file P90803k, 1st PRT with 1134 range samples.

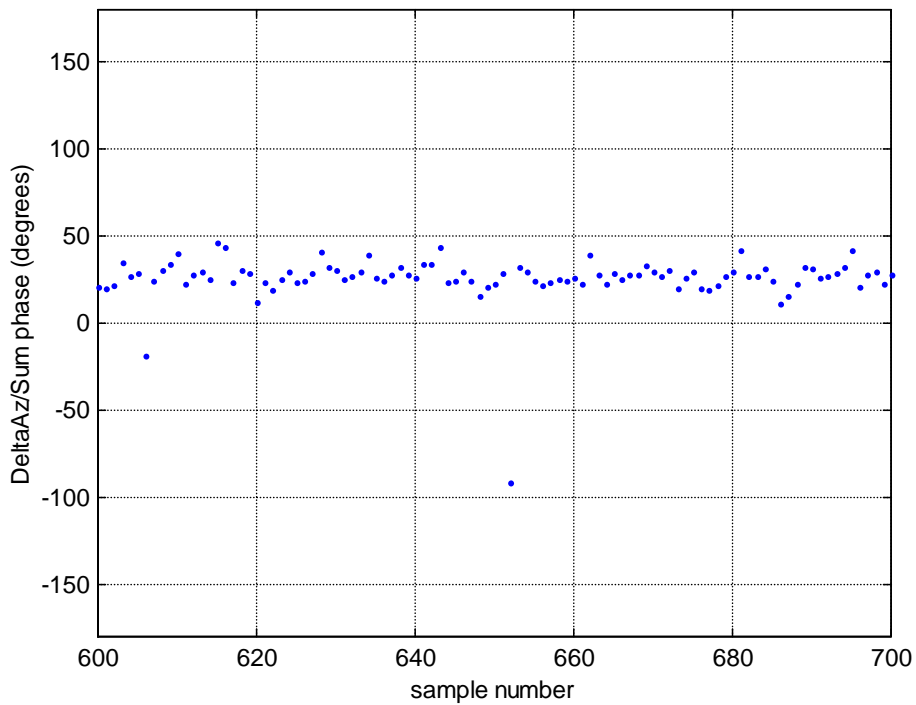


Figure 14.19. Phase of the ratio between the difference in azimuth and the sum beams; file P90803k, 19th PRT with 1134 range samples.

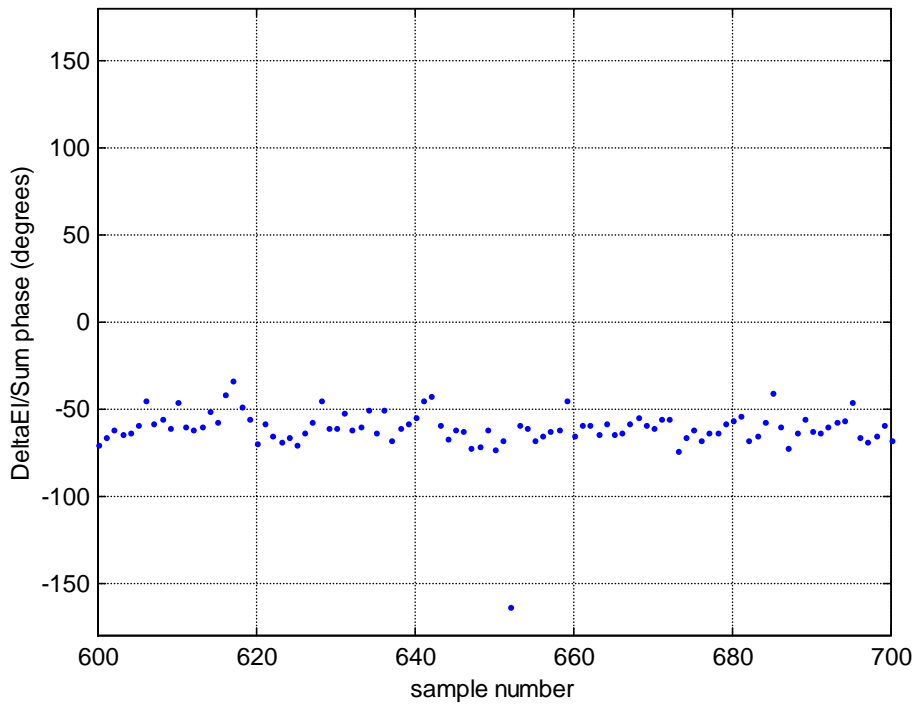


Figure 14.20. Phase of the ratio between the difference in elevation and the sum beams; file P90803k, 19th PRT with 1134 range samples.

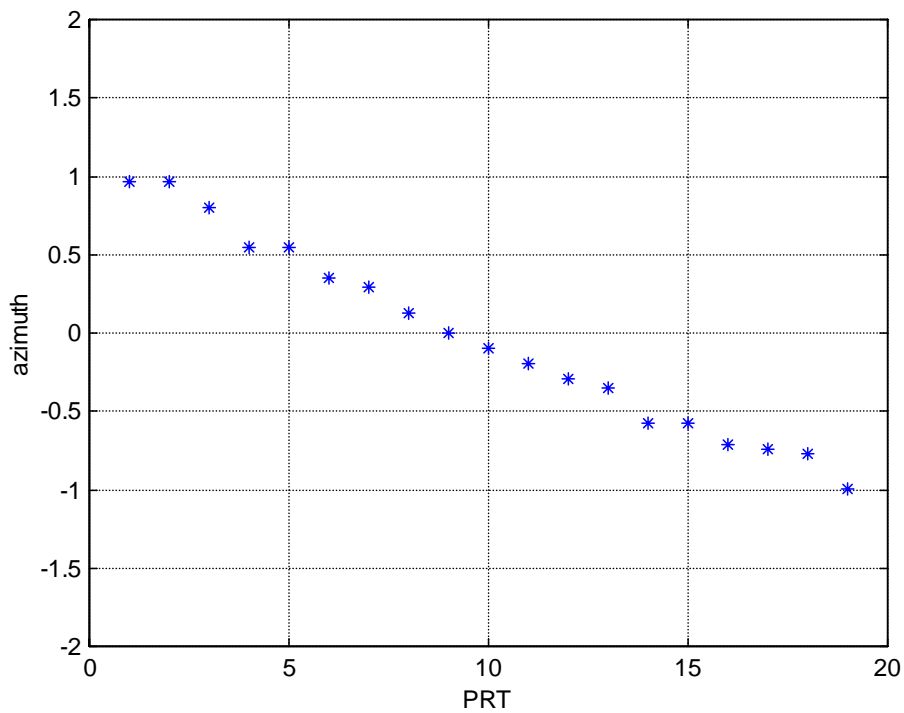


Figure 14.21. Estimate of the target azimuth; file P90803k, PRT with 1134 range samples, phase compensation.

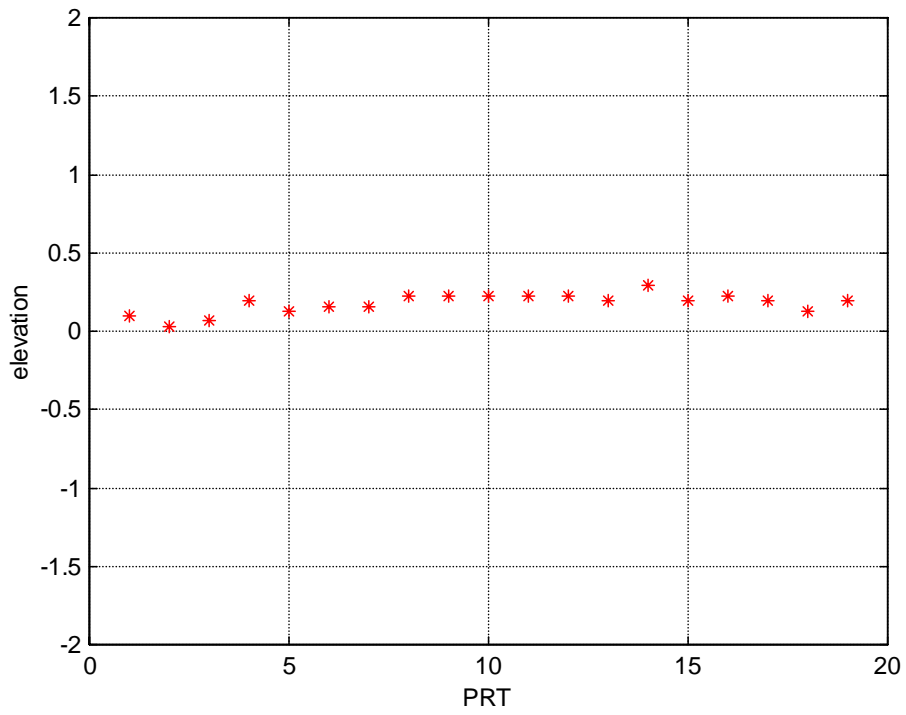


Figure 14.22. Estimate of the target elevation; file P90803k, PRT with 1134 range samples, phase compensation.

θ_T	ϕ_T	$\theta_T - \hat{\theta}_T$ (3 beams)	$\theta_T - \hat{\theta}_T$ (4 beams)	$\phi_T - \hat{\phi}_T$ (3 beams)	$\phi_T - \hat{\phi}_T$ (4 beams)	σ_θ (3 beams)	$CRLB_\theta$ (3 beams)	σ_θ (4 beams)	$CRLB_\theta$ (4 beams)	σ_ϕ (3 beams)	$CRLB_\theta$ (3 beams)	σ_ϕ (4 beams)	$CRLB_\theta$ (4 beams)
-1°	-1°	-0.01°	-0.01°	-0.08°	0.01°	1.27°	0.28°	0.24°	0.21°	1.31°	0.28°	0.23°	0.21°
-1°	0°	0.15°	0.03°	0.23°	0.03°	0.82°	0.24°	0.10°	0.08°	1.23°	0.77°	0.26°	0.25°
-1°	1°	-0.12°	0.02°	0.30°	0.02°	1.43°	0.26°	0.06°	0.06°	1.89°	1.16°	0.28°	0.26°
0°	-1°	0.14°	0.00°	0.06°	0.03°	1.28°	0.77°	0.27°	0.25°	0.90°	0.24°	0.08°	0.08°
0°	0°	0.18°	0.03°	0.11°	0.02°	0.79°	0.55°	0.09°	0.08°	0.78°	0.55°	0.08°	0.08°
0°	1°	-0.24°	0.02°	0.21°	0.01°	0.90°	0.50°	0.05°	0.05°	1.21°	0.69°	0.09°	0.09°
1°	-1°	0.47°	-0.01°	0.03°	0.03°	1.70°	1.16°	0.30°	0.26°	0.96°	0.26°	0.07°	0.06°
1°	0°	0.48°	0.01°	-0.19°	0.02°	1.50°	0.69°	0.09°	0.09°	1.12°	0.50°	0.06°	0.05°
1°	1°	0.20°	0.01°	0.05°	0.02°	1.21°	0.52°	0.06°	0.06°	1.07°	0.52°	0.06°	0.06°

Table 14.2 : Results of the MLE algorithm simulation; scenario consisting of a target with angular co-ordinates (θ_T, ϕ_T) and of a MBI with co-ordinates $(\theta_T, \phi_T) = (-1.5^\circ, -1.5^\circ)$; SNR=INR=30 dB; results averaged over 100 Monte Carlo trials; the target has been detected in all the trials.

List of acronyms

A/D	Analogue-to-Digital
C-PAR	C-band Phased Array Radar
CRI	Coherent Repeater Interference
CRLB	Cramer Rao Lower Bound
dB	decibel
FIM	Fisher Information Matrix
IE	Interference Emulator
INR	Interference-to thermal-noise power ratio
MBI	Main Beam Interference
MDDR	Multi channel Digital Data Recorder
MLE	Maximum Likelihood Estimation
NLI	Noise-Like Interference
PRT	Pulse Repetition Time
SLB	Sidelobe Blanker
SLC	Sidelobe Canceller
SNR	Signal-to thermal-noise power ratio
TDoA	Target Direction of Arrival
TP	Transponder